Rev.Adv.Mater.Sci. 5 (2003) 311-318

MECHANICAL PROPERTIES OF ZrO_2-Al_2O_3 NANOSTRUCTURED PVD COATINGS EVALUATED BY NANOINDENTATION

A. Portinha[1], V. Teixeira[1], J. Carneiro[1], S. N. Dub[2] and R. Shmegera[2]

[1] University of Minho - Physics Department, Campus de Azurém, 4800 Guimarães, Portugal
[2] Institute for Superhard Materials, Department No.11, 2 Avtozavodskaya St., Kiev, 04074 Ukraine

Received: June 11, 2003

Abstract. ZrO_2-Al_2O_3 thin nanostructured coatings and stabilised ZrO_2-Y_2O_3 coatings have been deposited by magnetron sputtering in rotating mode with two metallic targets in order to stabilise the high temperature phases of zirconia at room temperature.
The structural studies were carried out using X-Ray Diffraction (XRD). Scanning Electron Microscopy (SEM) and Atomic Force Microscopy (AFM) were used to characterise the coatings morphology and microstructure. It was shown that the tetragonal phase of Zirconia can't be stabilised in the coatings with 2 wt.% of Al_2O_3.
The mechanical behaviour of ZrO_2-Al_2O_3 thin films under point loading conditions was studied by nanoindentation using Berkovich indenter with 130 nm tip radius. Low load tests were used to study the effect of the deposition parameters on the hardness and elastic modulus of coatings. The hardness of the films reaches 15.3 GPa for a ZrO_2-Al_2O_3 nanostructured coating sputtered at -70V applied bias. High peak load tests were used to estimate the film adhesion to steel substrates; 120 mN peak load showed good adhesion properties of the film.
The residual stresses were also determined using the Stoney equation and the highest compressive residual stress was found to be about -3 GPa for the sample with highest hardness.

1. INTRODUCTION

Zirconia is a technological material that has lots of applications such as optical coatings [1], protective coatings at high temperatures [2-4], thermal barrier coatings [4], chemical sensors [5-6]. This makes Zirconia-based coatings a very interesting material for the next generation of coatings for wear resistant applications. ZrO_2 crystallizes in three distinct polymorphs depending on temperature and pressure conditions. It is well known that ZrO_2 monoclinic phase is stable at room temperature; the tetragonal phase is stable from 1170 to 2370 °C and cubic phase stability region is 2370-2680 °C [2, 7-11].

When the applications of the discussed coatings imply operations in a temperature range where the phase transformations occur, it is necessary to stabilise the high temperature phase at room temperature. It is due to the fact that phase transformation is typically accompanied by 3-5% volume expansion, which can produce high residual stresses and microcracks leading to delamination and spallation of coatings. Phase stabilization of ZrO_2 is usually provided by doping with other oxides such as Y_2O_3, CeO_2, MgO, CaO, and Al_2O_3 [2,7-13].

Alumina is knownn to possess a higher Young modulus than zirconia (390 Gpa, approximately twice than ZrO_2), so the stabilization of zirconia tetragonal phase is suggested to produce by forming a rigid matrix around the zirconia crystals, which causes a local compressive stress and hinders this mechanism of the martensitic phase transformation

Corresponding author: V. Teixeira, email: vasco@fisica.uminho.pt

[14]. This matrix can be in form of nanocomposite coating, where the zirconia nanocrystals are embedded in an amorphous alumina matrix or in a nanolaminated structure. In doing so one can improve the behaviour of the coatings at high temperatures where the diffusion barrier is important, as well as their corrosion and wear protection [12,13,15-17].

Magnetron sputtering is a deposition technique allowing a good control of the mechanical (hardness, elastic modulus, residual stresses, adhesion and so on) and physical properties, crystallinity, and adhesion of the coatings. In turn, this gives the opportunity to improve the behaviour of coatings during operation at room and/or higher temperatures [15-21].

Mechanical properties investigations had an important development in the last decade mainly due to the nanoindentation technique combined with finite element studies, which offers capabilities to measure hardness and elastic modulus of nanocoatings with a few nanometers thickness at room and high temperatures (400-500 °C) [22-29]. Note that this technique provides a possibility to evaluate mechanical properties in 'real' values, i.e. the influence of substrate material is eliminated since the maximum deep of indentations remains lower than 10-15% of the coatings thickness [30].

In this work we gave especial attention to the micro structural and mechanical characterization of ZrO_2-Al_2O_3 thin nanostructured coatings and coatings doped with Y_2O_3 through the XRD studies, residual stresses and nanoindentation measurements.

2. EXPERIMENTAL

Preparation. ZrO_2-Al_2O_3 nanostructured coatings and ZrO_2-Al_2O_3-Y_2O_3 coatings have been deposited by reactive magnetron sputtering in rotating mode at 4 rpm constant rotation speed with two metallic targets in order to stabilize the high temperature phases of zirconia at room temperature. DC and RF power supply were used for the zirconium and aluminum targets, respectively.

Steel, glass and Inconel 738 LC (Ni-alloy) were used as substrates. The alloy substrates were polished until 1 micron diamond suspension, and all substrates were ultrasonically cleaned before the deposition process. Both targets and substrates were pre-cleaned in argon atmosphere for 10 minutes. All coatings were deposited at constant target-substrate distance (60 mm). Table 1 presents the main deposition parameters.

Characterization. All coatings were examined by Scanning Electron Microscopy (SEM) and Atomic Force Microscopy (AFM) to characterise their morphology and microstructure. The chemical composition of the coatings was determined by Energy Dispersive X-Ray spectroscopy (EDX).

X-Ray diffraction (XRD) measurements with a powder X-ray diffractometer (Cu *K*α radiation) were

Table 1. Sputtering deposition parameters for $ZrO_2Al_2O_3$ and $ZrO_2Y_2O_3Al_2O_3$ coatings. Thickness and wt.% of Al_2O_3 and Y_2O_3.

	Sample Codes							
PARAMETERS	ZrAl2	ZrAl4	ZrAl6	ZrAl7	ZrAl8	Zr8YAl1	Zr8YAl2	Zr8YAl3
Current (A)					2.86			
RF Power for aluminium (w)	600	250	600	600	600	600	600	600
Base pressure (Pa)	$>10^{-4}$	10^{-4}	$6*10^{-5}$	$>10^{-4}$	$7*10^{-5}$	$2*10^{-4}$	$2*10^{-4}$	$2*10^{-4}$
Substrate temperature (°C)	250	250	350	350	100	250	250	250
% of O_2 Flux					20			
Work Pressure (Pa)					$6*10^{-1}$			
Bias voltage (V)		-50		-70	-50		-70	-100
Deposition time (s)	28800	34200	28800	14400	21600	36000	36000	36000
Thickness (nm)	1200	1540	1350	760	1280	1350	1200	1420
wt. % of Al_2O_3	9.1	1.7	5	9.1	9.1	14.6	14.6	14.6
wt. % of Y_2O_3	–	–	–	–	–	4.1	4.1	4.1

Table 2. Surface roughness, grain size, $I_{(200)}/I_{(111)}$ ratio and residual stresses.

Sample Codes	ZrAl2	ZrAl6	ZrAl7	ZrAl8	Zr8YAl1	Zr8YAl2	Zr8YAl3
Ra (nm)	5.81	7.56	4.51	7.52	13.69	–	–
Rms (nm)	7.4	9.46	5.69	9.32	17.22	–	–
Grain size (nm)	24.7	28.1	24.6	23.9	35.8	25.2	25.2
$I_{(200)}/I_{(111)}$	3.4	8.0	0.2	0.9	7.5	9.0	7.4
Residual Stresses σ (GPa)	-0.89	0.639	-3.401	0.584	-0.149	-0.254	-0.5

used to study the phase composition, preferential crystal orientation and grain size.

The mechanical properties were evaluated by nanoindentation with a Nano Indenter II (MTS Systems, Oak Ridge, USA) using Berkovich indenter. 5 indents were performed for each sample at three different loads (5 mN, 10 mN, and 30 mN). Indentations at 120 mN were performed for a qualitative evaluation of the adhesion.

Residual stresses were calculated using the Stoney equation after measuring the curvature radius before and after deposition with a laser beam.

3. RESULTS AND DISCUSSION

3.1. Coatings microstructure

Two different nanocomposite coatings based on stabilised zirconia are discussed in this work: ZrO_2 nanocrystaline grains in an amorphous alumina matrix and ZrO_2-Y_2O_3- Al_2O_3 mixed oxides.

All coatings had a transparent aspect after deposition. Film thickness, evaluated by SEM, is presented in Table 1. The microstructure is similar in all films: a dense columnar growth structure and a very smooth surface showing thin top columns were observed. However, few small hillocks were also observed; we consider them as being due to (i) the loose of atomic mobility during deposition; (ii) possible surface defects on the substrate that causes the imperfect growth of some columns; (iii) the high quantities of material sputtered as a result of the high currents used; and (iv) oxidation of the target surface (its break give rise to high remotion of material from target surface). The film semi quantitative composition determined by EDX is given in Table 1.

Fig. 1 demonstrates a typical tree-dimensional micrograph of the ZrAl7 sample (sputtered at 350 °C and -70 V as negative bias) obtained by AFM, surface nanomorphology can be seen and analysed here. Thin size of the top columnar growth, smooth and compact surface were attributed to the lower surface roughness (see Table 2).

A decrease in surface roughness is observed with the increase of substrate deposition temperature and with increase of the negative bias. This effect is due to the higher atomic mobility that improves the coalescence between grains and the higher structural densification improved by the bombardment during the film growth. Note that ZrO_2 - Y_2O_3 -Al_2O_3 coatings have higher roughness values [31].

3.2. Structural characterization

ZrO_2 is an interesting material and has many technological applications. However, for high temperature applications it is necessary to suppress the

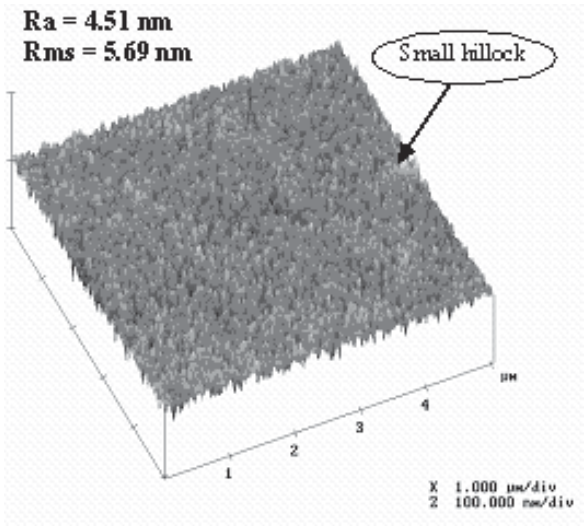

Fig. 1. Tree-dimensional AFM micrograph of a ZrAl7 sample (sputtered at 350 °C and bias -70V) illustrating the surface morphology.

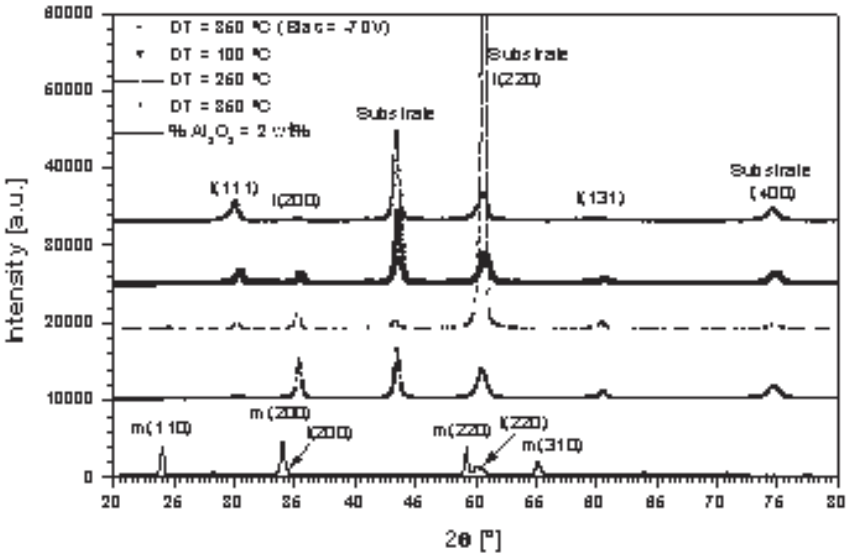

Fig. 2. XRD patterns for the $ZrO_2Al_2O_3$ nanostructured coatings.

tetragonal-to-monoclinic transformation and get the high temperature phases stabilised at room temperature. The transformation can be suppressed by alloying zirconia with trivalent oxides such as Y_2O_3, CeO_2, Gd_2O_3 and Al_2O_3 or retaining the crystallite grain sizes under the critical size (30nm) [15,32] constrained on an amorphous matrix like Al_2O_3.

To get the phase composition and other structural information, the coatings have been analyzed by XRD; Fig. 2 presents the XRD patterns for the $ZrO_2Al_2O_3$ nanostructured coatings. All coatings crystallize in the tetragonal phase, however, the main phase is monoclinic for the coating with 1.7 wt.% Al_2O_3. Other coatings were produced and the limit of Al_2O_3 percentage to stabilize ZrO_2 was found to lie between 2 and 5 wt.%.

When the substrate deposition temperature increases from 100 °C to 350 °C, significant changes in the nanocrystaline structure orientation are observed; as well as for changes in the applied negative bias. No preferential crystalline orientation was observed for the coating deposited at 100 °C, the ratio between the intensities of the two main diffraction directions (111) and (200) are ≈1. However, the increase in the deposition temperature leads to the preferential increase in the direction (200) and reduction of (111) direction. The ratio between the intensities of these two diffraction peaks is presented in Table 2. On the other hand, the increase in negative bias improves a preferential growth in the direction (111).

Monoclinic phase was not observed for the coatings doped with Y_2O_3 and Al_2O_3 at the negative bias changing from -50 V to -100 V. The preferential growth occurs in the (200) direction; no significant changes in the structural crystalline orientation were detected here. This fact follows from the small changes registered in the peaks intensities.

The main peaks were fitted using a Pseudo-Voigt function; the Gaussian and Lorentzian components (representing the micro strain and grain size, respectively [33]) were calculated for each peak. The grain size was determined by the Scherer equation (see Table 2). An increase in the deposition temperature increases the grain size due to the better atomic mobility and coalescence during the film growth. The increase in the negative bias reduces the grain size. The crystallite size of $ZrO_2Y_2O_3Al_2O_3$ coatings was higher than in the $ZrO_2Al_2O_3$ nanocomposite coatings under the same deposition conditions and reaches 36 nm.

3.3. Residual stresses

Residual stresses σ were calculated using the curvature radius [34] (measured with a micro-displacement-laser transducer) technique based on the Stoney equation [35]:

$$\sigma = -\frac{E_s t_s^2}{6(1-\nu_s)t_f} \times \left(\frac{1}{R_a} - \frac{1}{R_b}\right), \qquad (1)$$

where $E_s/(1-\nu_s)$ is the biaxial modulus of the substrate, t_s and t_f are the substrate and coating thickness respectively; R_a is curvature radius after deposition and R_b is the curvature radius before deposition. The residual stresses for the coatings are listed in Table 2; they are positive for coatings prepared at low temperature and negative for all other coatings; this means that there is a compressive state in the plane parallel to the surface. An increase in compressive residual stresses was observed for $ZrO_2Al_2O_3$ samples, however, the sample prepared at 350 °C shows a tensile stress that can be due to some relaxation after deposition. The highest compressive stress (-3.4 GPa) was observed for the sample deposited at -70 V bias and 350 °C. This implies a more densification of the film structure due to the bombardment by the working gas during deposition. In turn, some of these Ar ions can incorporate into the crystalline structure and increase the negative residual stresses. $ZrO_2Al_2O_3Y_2O_3$ coatings also demonstrate an increase in compressive stresses at higher applied negative bias.

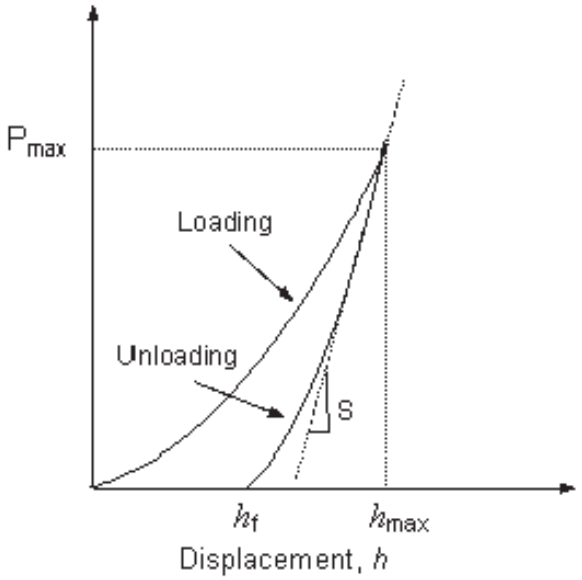

Fig. 3. Schematic representation of indentation load-displacement data during one complete cycle of loading and unloading.

3.4. Hardness and elastic modulus evaluated by nanoindentation measurements.

The indentation hardness is not a fundamental material property since it depends on the way it is determined (testing technique, evaluation, *etc.*). Despite of this, the indentation hardness is widely used as a parameter characterizing the mechanical properties of materials, in particular of metals, for several reasons: indentation hardness tests are relatively easy to perform; they provide a value that gives a direct measure for loading – bearing capacity of the investigated material. Moreover, for completely plastic contacts, the hardness of the material also gives an indirect measure of its uniaxial tensile yield stress [36].

$$H = c\,\sigma_y, \tag{2}$$

where c, the constraint factor, depends on the ratio E/σ_y of the material. For most metals, for which $E/\sigma_y \geq 100$, the constraint factor has a value of $c \approx 3$ [36]. Another reason for the widespread application of hardness tests is closely related with the definition of indentation hardness as a *local* measure of the mechanical properties.

In this work the hardness and elastic modulus were calculated using Berkovich nanoidentation measurements. The physical principles and models used to determine H and E from indentation load – displacement data are based on the Oliver–Pharr theory [22].

A schematic representation of indentation load (P) versus displacement (h) data obtained during a one full cycle of loading and unloading is presented in Fig. 3. The important quantities are the peak load (P_{max}), the maximum depth (h_{max}), the final or residual depth after unloading (h_f), and the slope of the upper portion of the unloading curve ($S=dP/dh$). The parameter S is known as the elastic contact stiffness. The hardness and elastic modulus can be derived from these values. The continuous stiffness measurement technique is used to monitor the average contact pressure (ACP) for loading segment. To monitor the average contact pressure in the indent during the indenter reloading, the procedure suggested in [23] was used.

The fundamental relations to calculate H and E are:

$$H = \frac{P_{max}}{A}, \tag{3}$$

where A is the projected contact area at that load, and:

$$E_r = \frac{\sqrt{\pi}}{2}\frac{S}{\sqrt{A}}, \tag{4}$$

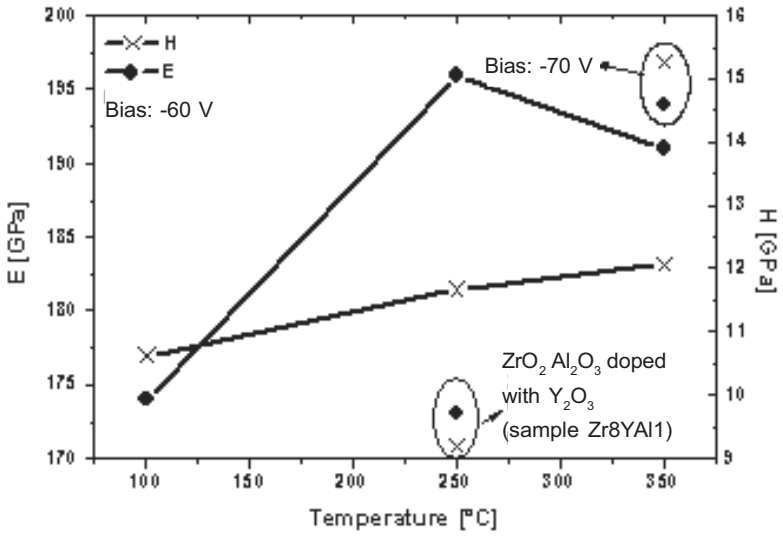

Fig. 4. Hardness and Elastic Modulus values function of deposition parameters for tests performed at 5 mN maximum load.

where E_r is the reduced elastic modulus which accounts for the fact that elastic displacements occur in both indenter and sample. The elastic modulus of the test material, E, is calculated from E_r using:

$$\frac{1}{E_r} = \frac{1-\nu^2}{E} + \frac{1-\nu_i^2}{E_i}, \qquad (5)$$

where ν is the Poisson's ratio for the test material, and E_i and ν_i are the elastic modulus and Poisson's ratio of the indenter, respectively. The elastic constants E_i = 1141 GPa and ν_i=0.07 are often used for a diamond [37]. Eq. (2) is a working definition for the hardness. By this definition, hardness a measure of the load – bearing capacity of the contact computed by the applied load divided by the *projected area of contact under load*. The most widely used method to establish this contact area was suggested in Oliver – Pharr theory [36].

Fig. 4 demonstrates the values of hardness (H) and elastic modulus (E) extracted from the loading-unloading curves from the tests performed at 5 mN (high load peak) to assure no substrate influence in the retrieved data.

These results show an increase in the hardness values with deposition temperature and higher applied bias. The highest value reaches 15.3 GPa for the sample prepared at 350 °C and -70V bias. Similar results were obtained for the elastic modulus. The value for elastic modulus is almost constant for the samples prepared at 250 °C and 350 °C as well as for the sample prepared at -70V bias. The sample doped with Y_2O_3 presents lower values of hardness and elastic modulus.

The mean values of H and E for three different test sets performed at different maximum loads (5, 10, and 30 mN) are listed in Table 3. All samples have a similar behaviour, which is characterized by

Table 3. Hardness and elastic modulus for various indentation loads.

	Properties (GPa)					
	Hardness (*H*)			*Elastic modulus* (*E*)		
Test Load (mN)	5	10	30	5	10	30
ZrAl2	11.7	9.65	6.83	196	182	162
ZrAl6	12.1	11.8	8.6	191	190	179
ZrAl7	15.3	12.6	6.4	194	185	157
ZrAl8	10.6	10.7	6.0	174	178	147
Zr8YAl1	9.19	8.15	7.16	173	168	165

the decrease in *H* and *E* values with increase in maximum peak load. This effect is explained by the contribution of substrate because the measurements at higher loads have promoted indentation deeps superior than 10-15% of coatings thickness; these values reaches about 1/3 of the total thickness in the case of 30 mN. As follows from the analysis of the results obtained for the sample ZrAl7, the increase in hardness and residual stress with temperature can be due the higher densification of nanocoatings structure. Hardness was also shown to be related with grain size and surface roughness. The hardness increases for lower grain size, this fact is in agreement with other studies and is attributed to the increase in the number of grain boundaries, which, in turn, increases the surface energy and reduces dislocations.

Analysing the surface roughness, we should emphasise that hardness increases as roughness decreases, since the higher hardness implies worth surface compactness, so the top of the columnar growth is freer and permits higher dislocations during indentation. The value of the maximum hardness of 15.3 GPa is in agreement with the relations presented before, because this sample has the higher compressive residual stresses, lower grain size and lower roughness.

The adhesion was evaluated qualitatively performing nanoindentation measurements at higher loads (120 mN); delamination of the coatings from the substrate was not observed.

4. CONCLUSION

We have grown nanocomposite sputtered coatings of zirconia and alumina, zirconia, yttria and alumina using metallic targets to stabilize the tetragonal phase of zirconia. The possibility to control at an atomic level and the addition of these elements to the zirconia matrix was shown for the stabilized zirconia deposition. Thus, the improved uniformization of the crystalline phases in the coating is obtained.

All coatings have a dense columnar structure and are transparent. Alumina stays amorphous in all coatings, while crystalline phases were detected for zirconia ((200) tetragonal direction is the predominant one). Monoclinic phase have been shown to be predominant in $ZrO_2Al_2O_3$ coatings with 2wt.% of Al_2O_3.

The increase in the deposition temperature dive rise to the increase in the grain size, while the increase in the negative bias value leads to the opposite effect.

Hardness and elastic modulus were determined by nanoindentation; an increase in their values was observed for higher deposition temperatures and higher negative bias. The hardness of the films reaches 15.3 GPa for a $ZrO_2Al_2O_3$ nanostructured coating deposited at bias -70V and temperature of 350 °C. Delamination of the films from substrate was not observed in the tests at 120 mN peak load. The compressive residual stresses in the coatings increase with deposition temperature and with negative bias. The hardness increase with the compressive residual stresses, decrease in roughness values and with decrease in the grain size.

ACKNOWLEDGEMENTS

This work was partially financially supported by FCT-Fundação para a Ciencia e Tecnologia-FCT under the project POCTI/EME/39316/2001: 'PVDCOAT-Composite and multilayered protective coatings for efficient energy systems'. A. Portinha is gratefully for the Research Grant supported by F.C.T.- Portuguese Foundation for Science and Technology.

REFERENCES

[1] T. Sikola, J. Spousta, L. Dittrichova and I. Benes // *Nucl. Instr. Methods Phys.B* **1 (**1999) 673.

[2] V. Teixeira and M. Andritschky // *High Temperature-High-Pressures* **25 (**1993) 213.

[3] V. Teixeira, M. Andritschky, W. Fischer, H.P. Buchkremer and D. Stöver // *Surf. Coat. Tech.* **120-121** (1999) 103.

[4] C. Funke, J.C. Mailand, B. Siebert, R. Vassen and D. Stöver // *Surf. Coat. Tech.* **94-95** (1997) 106.

[5] G. Z. Cao, H. W. Brinkman, J. Meijerink, K. J. Vries and A. J. Burggraaf // *J. Am. Ceram. Soc.* **76** (1993) 2201.

[6] J. Zosel, F. Blauwe and U. Guth // *Adv. Eng. Mater.* **3** (2001) 797.

[7] J.S. Kih, H.A. Marzouk and P.J. Reucroft // *Thin Solid Films* **254** (1995) 33.

[8] R. Guinebretiere, B. Soulestin and A. Douger // *Thin Solid Films* **319** (1998) 197.

[9] C.R. Aita, M.D. Wiggins, R. Whig and C.M. Scanlan // *J. Appl. Phys.* **79** (1996) 1176.

[10] Z. Ji, J.A. Haynes, M.K. Ferber and J.M. Rigsbee // *Surf. Coat. Tech.* **135** (2001) 109.

[11] P. Gao, L.J. Meng, M.P. Santos, V. Teixeira and M. Andritschky // *Thin Solid Films* **377** (2000) 32.

[12] J. D. Deloach, C. R. Aita and C.–K. Long // *J. Vac. Sci. Technol. A* **20** (2002) 1517.
[13] V. Teixeira, A. Monteiro, J. Duarte and A. Portinha // *Vacuum* **67** (2002) 477.
[14] S.B. Quadri, C.M. Gilmore, C. Quinn, E.F. Skelton and C.R. Gosset // *J. Vac. Sci. Technol*. *A* **7** (1989) 1220.
[15] R.C. Garvie // *J.Phys. Chem.* **82** (1978) 218.
[16] C.R. Aita // *Surface Engineering* **14** (1988) 421.
[17] P. Gao, L.J. Meng, M.P. Dos Santos, V. Teixeira and M. Andritschky // *Vacuum* **64** (2002) 267.
[18] R. Brenier and A. Gagnair // *Thin Solid Films* **392** (2001) 143.
[19] J.P. Holgado, J.P. Espinós, F. Yubero, A. Justo, M. Ocańa, J. Benítez and A.R. González-Elipe // *Thin Solid Films* **389** (2001) 34.
[20] L. Bianchi, A.C. Leger, H. Vardelle, A. Vardelle and P. Fauchais // *Thin Solid Films* **305** (1997) 35.
[21] K. Goedicke, J. Liebig, O. Zywitzki and H. Sahm // *Thin Solid Films* **377-378** (2000) 37.
[22] W.C. Oliver and G.M. Pharr // *J. Mater. Res*. **7** (1992) 1564.
[23] S. Dub, N. Novikov and Y. Milman // *Phil. Mag. A* **82** (2002) 2161.
[24] B. D. Beake and J. F. Smith // *Phil. Mag. A* **82** (2002) 2179.
[25] C. Louro, A. Cavaleiro, S. Dub, P. Smid, J. Musil and J. Vlcek // *Surf. Coat. Tech.* (2002), in print.
[26] G.M. Pharr and W.C. Oliver // *J. Mater. Res*. **17** (1992) 28.
[27] Mingwu Bai, Koji Kato, Noritsugu Umehara and Yoshihito Miyake // *Thin Solid Films* **377-378** (2000) 138.
[28] R. M. Souza, G.G.W. Mustoe and J.J. Moore // *Thin Solid Films* **355-356** (1999) 303.
[29] R. M. Souza, G.G.W. Mustoe and J.J. Moore // *Thin Solid Films* **392** (2001) 65.
[30] J.V. Fernandes, A.C. Trindade, L.F. Menezes and A. Cavaleiro // *J. Mater. Res*. **17** (2000) 1766.
[31] C.V. Thompson // *Annu. Rev. Mater. Sci.* **30** (2000) 159.
[32] R.C. Garvie // *J.Phys. Chem.* **69** (1965) 1238.
[33] Th. H. De Keijser, J. I. Langford, E. J. Mittemeijer and A. B. P. Vogels // *J. Appl. Cryst.* **15** (1982) 308.
[34] M. Larson, P. Hedenqvist and S. Hogmark // *Surface Eng.* **12** (1996) 43.
[35] M. Larson, M. Bromark, P. Hedenqvist and S. Hogmark // *Surf. Coat. Tech.* **76/77** (1995) 202.
[36] T.H. Courtney, In: *Mechanical Behaviour of Materials* (McGraw-Hill, New York, 1990).
[37] G.M. Pharr and W.C. Oliver // *MRS bulletin*, July 1992.